International Journal of Applied Pharmaceutics

ISSN- 0975-7058 Vol 16, Issue 5, 2024

Original Article

DEVELOPMENT OF NANOSPONGES-BASED TOPICAL FORMULATION FOR THE EFFECTIVE DELIVERY OF SELECTED ANTIFUNGAL DRUG

RUDROJU ANUSHA, MOTHILAL M.*

Department of Pharmaceutics, SRM College of Pharmacy, SRM Institute of Science and Technology, SRM Nagar, Kattankulathur, TamilNadu-603203, India

***Corresponding author: Mothilal M.; *Email: mothipharma78@gmail.com**

Received: 16 May 2024, Revised and Accepted: 24 Jul 2024

ABSTRACT

Objective: To increase luliconazole's therapeutic impact, distribution, and preservation, this project is aimed to prepare cyclodextrin-based nanosponge gel and test its topical skin administration.

Methods: The convection heating method produced cyclodextrin-diphenylcarbonate nanosponges, which later loaded with luliconazole by freeze-drying. Response Surface Methodology (RSM) was used to examine the association between procedure parameters and quality variables. Pilot study findings were analyzed using Analysis of variance. Key technique factors affect quality metrics in contour, RSM, and perturbation graphs.

Results: The mean medication payload was 42.19±1.45 mg of luliconazole/g of lyophilized powder. The remarkable encapsulation efficiency of luliconazole (90.12±0.92%) supports an inclusion complex. Laser light scattering evaluation of luliconazole-loaded-nanosponges shows an unimodal and narrow particle size distribution of 60-73 nm. Drug encapsulation does not change a typical nanosponge's spherical form, according to microscopic investigations. Physico-chemical characterized verified the nanosponge-luliconazole inclusion complex. The complex release is faster than pure medication *in vitro*. Pure luliconazole dissolves 12% in 12 h, whereas nanosponge encapsulated medicine is absorbed faster and better. After 12 h, nanosponge formulations released 93-95% luliconazole. A model carbopol gel formulation with nanosponge formulations examined skin permeability, antifungal effectiveness, and stability. In 12 h skin permeation trials, nanosponge-encapsulated luliconazole leaked slowly across rat skin.

Conclusion: The slow drug release, greater skin penetration, and superior storage stability of the gel formulation based on cyclodextrin nanosponges of luliconazole imply that it has great potential as a topical delivery system.

Keywords: Luliconazole, Response surface methodology, Nanosponges, Freeze drying, Inclusion complex, Skin permeability

DOI: https://dx.doi.org/10.22159/ijap.2024v16i5.51466 Journal homepage: https://innovareacademics.in/journals/index.php/ijap

INTRODUCTION

Luliconazole (LU), an optically active imidazole antifungal, treats superficial mycoses in dermatology. Tokyo-based Nihon Nohyaku Co. Ltd. makes it. Notably, it has extensive antifungal efficacy against pathogenic fungi, especially dermatophytes. After its 2005 debut in Japan, liconazole is now accessible as 1% creams and solutions to treat superficial infections like dermatophytoses, candidiasis, and pityriasis versicolor. LU inhibits fungal cell wall formation by restricting the conversion of lanosterol to ergosterol by the CYP450 14-α-demethylase enzyme [1-4].

The drug is very permeable and poorly water-soluble. The product is safe and effective against most dermatophytes, with a minimal inhibitory concentration (MIC) of 0.004-0.008µg/ml and low toxicity [5]. The pKa and water solubility of LU are 6.34 and 0.0659 mg/ml, respectively. Its limited water solubility limits cutaneous availability and topical administration. Drug solubility in the stratum corneum lipid layer limits the penetration rate. Topical fungal infection treatment must be localized in dermal and epidermal layers [6]. Conventional and commercial formulations have low skin penetration and drug retention. Various methods have been tried to improve topical antifungal delivery. Permeation enhancers can cause systemic toxicity. Nanosponges (NS) and microemulsion-based gels have been studied by several researchers. Manish *et al.* improved solubility and antifungal efficacy with LU nanocrystals-loaded hydrogel. Vivek *et al.* found that herbal ethosomal gel increased the cutaneous distribution of LU. Manjot *et al.* made LU vesicular gel for topical administration [7-9].

Drug solubility, stability, and efficacy have been improved by chemical modification of antifungal drugs and carrier-based administration using penetration enhancers, nanoformulations, iontophoresis, photodynamic therapy, and lasers. Triazole-containing formulations may differ in stability and solubility during storage. Some formulas discolor after 1 or 2 d, becoming yellow to deep red or brown. This may deter individuals from taking prescribed medications [10, 11]. Dermatomycoses are surface fungal infections that are frequent in our practice and worldwide. Dermatophyte fungus from humans or animals causes these infectious disorders. Topical antifungal therapy's efficacy depends on its SC penetration and duration [12].

Another medication solubility and stability enhancer is Cyclodextrin (CD). Research studies state that sulphoalkylether CD derivative molecular encapsulation boosts LU's water solubility. Sulphobutyl-substituted β-CD derivatives. Unmetabolized CD may be poisonous and unsuitable as a medicinal excipient. CDs cannot host inclusion complexes because the complex dissociates quickly on dilution and the guest molecules' polarity and size restrictions preclude hydrophilic or high-molecular-weight compounds from complexing. Thus, a ready-to-use LU formulation with better aqueous stability over storage is needed [13, 14].

Over the past decade, Cyclodextrin Nanosponges (CDNS) have become a drug delivery platform for difficult-to-synthesize molecules. Recently developed NS are three-dimensional networks of hyper cross-linked CD polymers. Polymers are generated by reacting CD with cross-linkers such as carbonyldiimidazole or diphenyl carbonate. CDNS complexed more molecules than natural ones. They protect labile groups, improve solubility, and limit weakly soluble active release [15-17]. CDNS enhanced curcumin solubility and decreased hydrolytic breakdown and biotransformation, according to Darandale and colleagues [18].

Screening investigations found critical technique factors (process and formulation variables) affecting critical quality features (performance characteristics). A Decisive Screening Design (DSD) was chosen above various response surface designs to optimize crucial technique parameters. Recently developed, enriched three-level designs, DSD, provide well-organized main effect estimates that are unbiased to quadratic effects and two-factor interactions. DSD

avoids confounding, can identify nonlinear or curvilinear response components, and may eliminate the need for follow-up tests. The DSD evenly samples the parameter space, allowing all secondary interactions to be explored with little aliasing. Its experimental requirements rise linearly with parameter addition. These benefits make it helpful for investigations with quadratic effects and undefined secondary interactions [19].

Consequently, the purpose of this research was to find out if LU's chemical stability and water solubility might be enhanced using NS made of CD.

MATERIALS AND METHODS

Materials

We synthesized CD-based carbonate NS in our laboratory, as documented in a previous publication [20]. LU was supplied by Hetero Labs in Hyderabad. S. D. Fine Chem. Pvt. Ltd., based in Mumbai, provided carbopol 934, methanol, propylene glycol, phosphotungstic acid, triethanolamine, chloral hydrate, Tween80, sodium chloride, agar, dextrose and N-methyl-2-pyrrolidone. The Milli-Q®RO system's built-in water supply was used for the execution of the moveable solvent system and washing solutions. Wistar Albino rats were procured from Vab Bioscience, Hyderabad.

Methods

Solubilization efficiency of NS

This study examined NS (NS1-NS10)'s solubilization-enhancing potential and efficacy. NS (100 mg) and LU (≈200 mg) were combined and suspended in 20 ml Milli-Q water. A mechanical shaker mixed the volumetric flask contents at room temperature. To extract free LU from colloidal supernatant, the solutions were centrifuged at 10,000 RPM for 10 min after 24 h of equilibrium. Adding 10 ml of methanol to the mixture above extracted the NS' LU from the supernatant. Following this, a calibration curve was used to test the colloidal supernatant solution by Ultraviolet (UV) spectrophotometer at 294 nm.

Preparation of LU loaded β-CDs

A mechanical stirrer was used to suspend the NS in Milli Q water. To inhibit aggregation, 200 mg of LU was added and sonicated for 20 min. Then this mixture was stirred continuously for a set duration. The uncomplexed medicine was separated from the suspensions by centrifuging them at 5000 rpm for 20 min. The colloidal supernatant was lyophilized at-20 °C and 13.33 mbar to freeze dry. A desiccator kept the dry powder after lyophilization. All batches were analyzed for particle size, drug loading, and EE. Based on the NS type, luliconazole-loadedNSformulations were abbreviated as LUNS [21].

Design of experiments

The individual and interaction effects of essential technique parameters were examined utilizing a four-factor, three-level definitive screening approach. Using Design Expert® software, thirteen experiments were created and run while holding other factors like container volume, NS, and drug constant. Response surface methodology (RSM) examined how critical technique parameters affected critical quality attributes (CQAs). The trial experiment findings were analyzed using Analysis of Variance (ANOVA). Perturbation, RSM, and contour plots show how critical method parameters affect critical quality aspects [22, 23]. The quadratic effect of all important method parameters on each critical quality attribute was characterized by a polynomial prediction model. Equation 1 is the general representative polynomial.

$$Y = \beta_0 + \beta_1 X_1 + \beta_2 X_2 + \beta_3 X_3 + \beta_{12} X_1 X_2 + \beta_{13} X_1 X_3 + \beta_{23} X_2 X_3 + \beta_{11} X_1^2 + \beta_{22} X_2^2 + \beta_{33} X_3^2 \ldots \ldots (1)$$

Y-Analytical response

X_1, $X_2$and X_3-Critical method parameters

X_1X_2, $X_1X_3$and X_2X_3-Interaction terms

X_1^2, $X_2^2$and X_3^2-Quadratic terms

β_0-A constant

β_1, β_2 and β_3-Coefficients of individual effects

β_{12}, β_{13} and β_{23}-Coefficients of interactive effects

β_{11}, β_{22} and β_{33}-Coefficients of quadratic effects

Optimization

The ideal points for the independent variables were found via numerical optimization by restricting response parameters and affecting factors. To validate the optimization process, the nanoformulation was synthesized in triplicate under ideal circumstances.

Method operable design space

In the design space, crucial method parameters are changeable enough to yield satisfactory results. Within the design space, the technique will be robust. There are several ways to create design space. The design space is usually shown by contour plots of fitted responses. Design space is created by input factor combinations and reciprocity [24]. Design space was created using contour graphs. The design space is created by constraining important technique parameters.

Characterization of prepared LUNS

Particle size, polydispersity index (PDI), and zeta potential (ZP)

Dynamic Light Scattering (DLS) revealed LUNS' particle size distribution. The measurements were done at 90° for all samples. The samples were diluted with Milli Q water before testing. After averaging three data, cumulant analysis computed the particles' mean hydrodynamic diameter and PDI. An extra electrode in the same equipment measured ZP. All studies were done in triplicate at 25±2 °C.

Drug payload and encapsulation efficiency (EE)

EE is the ratio of drug weight entrapped in a carrier system to drug added. Drug loading is drug weight/carrier system weight [25]. To assess the concentration, the LUNS complex was dissolved in methanol, sonicated for 10 min to break it, diluted, and then examined using a UV spectrophotometer at 294 nm. The "percent drug payload" and "percent drug EE" were computed using equations 2 and 3:

$$\%\ \text{Drugpayload} = \frac{\text{Weight of drug encapsulatedin NS formulation}}{\text{Weight of the NS formulation taken for analysis}} \times 100 \ldots (2)$$

$$\%\ \text{Drugencapsulationefficiency} = \frac{\text{Weigh to f drug encapsulatedin NS formulation}}{\text{Initial weight of the drug fedfor loading}} \times 100 \ldots (3)$$

Transmission electron microscopy (TEM)

The morphology of both plain and LUNS was assessed using TEM. To enhance contrast, a film-coated copper grid was stained with a 2% (w/v) phosphotungstic acid aqueous solution using one drop of diluted nanoparticle suspension. The grid was then left to dry. Under TEM's 45000 magnification, the samples were examined.

Fourier-transformed infrared (FTIR) spectroscopy

The Tensor 27 FTIR was utilized to know the FTIR spectra of β-CD, plain NS, LU, physical mixture, and LUNS using the potassium bromide disc method from 4000 to 600 cm.

Differential scanning calorimetry (DSC)

DSC based on The FTIR spectra of various substances were examined using a Perkin Elmer DSC/7 differential scanning calorimeter (Perkin-Elmer, CT-USA) with a TAC 7/DX instrument controller. The substances included β-CD, plain NS, LU, physical mixed, and loaded NS. The melting point and fusion heat of the device were calibrated using indium. The temperature range of 30-400 °C was raised at a rate of 10 °C per min. The aluminum sample pans used were from Perkin-Elmer, and an empty pan served as a reference. Under nitrogen purge, three replicate analyses were performed on 5 mg samples.

X-ray powder diffraction (XRPD)

LU, plain, and loaded NS were analyzed using a Bruker D8 Advance X-ray diffractometer at a scan rate of 5°/min in the 2θ range of 2.5° to 60°.

In vitro release study

Multi-compartment (n=6) rotating cells with dialysis membranes were employed in *in vitro* release investigations. It contained 20 mg LU in 100 ml pH 6.4 buffers. Similar receptor media. After set time intervals, the receptor phase was diluted with distilled water and UV spectrophotometer-analyzed at 294 nm. Multiple experiments were done. By incorporating kinetic model fittings into dissolution study data, the drug release mechanism was evaluated.

Preparation of gel formulation of luliconazole nanosponges (LUNS)

LUNS gel basis was made with carbopol 934 [26]. A consistent 1% w/w gel was created by steeping the polymer in water for 2 h and then dispersing it in distilled water with a magnetic stirrer. The gel base was mixed with 1% triethanolamine, 2% N-methyl-2-pyrrolidone, and 2% w/w propylene glycol. After adding NS loaded with LU to the gel basis, the concentration reached 1% w/w (a drug-to-carrier ratio of 1:99). Free LU was added to the gel base to make the control.

Evaluation of gel formulations

pH determination

Gel pH was monitored with digital pH meters. 0.25 g NS-based gel was carefully weighed and mixed in 25 ml filtered water. Before use, pH 4.0, 7.0, and 9.0 buffer solutions calibrated the pH meter. Formulation pH was measured three times and averaged.

Skin permeation studies

The Central Animal House of TRR College of Pharmacy, with approval number 1447/PO/Re/S/11/CPCSEA-67/A, Hyderabad, India, provided 120–150 g 6–8 w old Wistar Albino rats for *in vitro* permeation studies. Animals lived in ventilated 25 °C chambers with a 12/12 light/dark cycle. Animals acclimatized for a week before testing. All animal experiments were authorized by the TRR College of Pharmacy institutional animal ethics committee. Both NS-encapsulated and free LU gels were given to three groups of rats.

In vitro skin permeation and deposition studies

The abdominal hair of Wistar Albino rats was carefully shaved after chloral hydrate anesthetized them. Subcutaneous fat, connective tissue, and 5 cm^2 abdominal skin were removed. Cleaning and defect inspection followed skin removal. *In vitro* skin permeation and deposition studies used Franz diffusion cells with a 3.14 cm^2 effective diffusion area. Excised dorsal skin samples were clamped between Franz diffusion cell donor and receptor chambers, stratum corneum side facing donor. The stratum corneum was thinly covered with 0.05 g of test gel having a 1 cm^2 diffusional area. A sink for skin penetration was created by adding 20 ml of physiological saline (pH 7.2) with 1% Tween80 to the receptor compartment, which increased the solubility of LU to 155.8 µg/ml. All through the experiment, the diffusion cells were mixed at a temperature of 32±1 °C while being spun at 300 rpm. At 0.5, 1,2,4,6,8,10, or 12 h, the receptor medium was removed and replaced with a new physiological saline solution to keep the sink conditions constant for each experiment. LU concentration was measured using High-Performance Liquid Chromatography (HPLC).

The skin was cleaned with distilled water at hours 3, 6, 9, and 12 after dorsal application to detach excess formulation. To remove the stratum corneum LU, the cellophane sticky tape was used to peel the epidermal layer. Sections of homogenized skin were cut. Methanol homogenized skin and extracted LU from tape. After centrifuging at 4000 rpm for 10 min, HPLC measured LU in the supernatant [27-29].

In vivo permeation study in mice

The dorsal hair was shaved and washed with a physiological solution (0.9% sodium chloride solution) 24 h before the experiment. Test gel (0.05 g) was thinly coated on the dorsal surface (3.14 cm^2). After the mice died at 3, 6, 9, and 12, the treated skin was dissected. The mice died from cervical dislocation. The same procedures were employed to treat methanol-extracted LU from skin samples. LU was measured in the epidermis and dermis using HPLC [27].

Assessment of anti-fungal activity

Candida albicans and *Aspergillus fumigatus* were investigated for NS-encapsulated LU effectiveness. Nutritional agar was autoclaved at 121 °C for 15 min from saboured dextrose in hot distilled water. Nutrient agar was evenly planted with 10 CFU/ml of test organisms [30]. Nutrient agar petri plates received aliquot test samples. After 30 min, plates were incubated at 25 °C for 24 h. *Candida albicans* and *Aspergillus fumigatus* zone of inhibition diameters were measured after 24 h.

Stability studies

Stability testing was performed on carbopol gels with free or NS-encapsulated LU (1%, w/w). Formulations were stowed in closed amber glass bottles at 25 °C±2 °C, 60% RH±5% RH, in a dark atmosphere. Aliquots (40–50 mg) were inserted in calibrated flasks at appropriate times (20 ml). Sonicated in methanol, diluted, membrane-filtered, and HPLC-analyzed for residual LU. We measured three times.

Statistical analysis

Each experiment had at least three trials. Statistics were compared using SPSS 12.0. Data are presented as means with standard deviations (mean S. D.), and statistical significance is indicated by a P value of 0.05.

RESULTS AND DISCUSSION

A new nanoscale polymer delivery technique, CDNS, may carry parenteral, oral, ophthalmic, and topical medicines. They enhance stability, permeability, bioavailability, and drug release. Hydrophilic and lipophilic substances are trapped in their porous structure. CDNS are innovative cross-linked cyclodextrin polymers nanostructured within a three-dimensional network. This type of cyclodextrin polymer can form porous insoluble nanoparticles with a crystalline or amorphous structure and spherical shape or swelling properties [31].

The gels and creams may contain NS. Effective penetration is needed for topical medication administration. Resveratrol-loaded NS boosted drug penetration in pig skin *in vitro*. Swaminathan S *et al.* (2010) found that rabbit buccal mucosa increased resveratrol permeability [32]. Thus, CDNS can topically distribute LU.

We made and examined ten NS (NS1-NS10) for this study. Pre-treated drug-loaded NS produced nanoparticles below 150 nm. All ten NS were compared to free LU in distilled water for solubilization. In fig. 1, all NS (NS1-NS10) increased solubility. The aqueous and lipid solubility characteristics of a drug substance are of fundamental importance in determining whether it is capable of reaching sites of absorption, its interaction with putative therapeutic targets and its ultimate metabolism and excretion. From the results it was evident that NS5 and NS6 are more soluble than the remaining NS. Due to matrix entrapment and drug inclusion complex formation, NS may solubilize better.

Freeze-drying loaded LU onto different NS. The drug-loaded NS formulations were named LUNS1–LUNS10, depending on the NS type. During drug loading, important parameters determining the quality of drug-loaded NS were found. Particle size (R1), percent drug payload (R2), and EE (R3) were significant quality features from preliminary scouting. Critical process parameters (CPPs) were cross-linking ratio (A), solvent volume (B), stirring speed (C), and stirring duration (D). The-1 and+1 crucial process parameters were optimized using the design of experiments. The definitive screening design randomly assigned thirteen experiments and used RSM to assess the data. Table 1 shows the experimental matrix and answers. Table 2 summarises design model statistics. All models were significant with large F-values. Multiple linear regression analysis provided polynomial equations for all essential quality indicators (table 3). Table 4 shows the mean, SD, R2, Adjusted R2, Predicted R2, Adeq Precision, and % CV of all models.

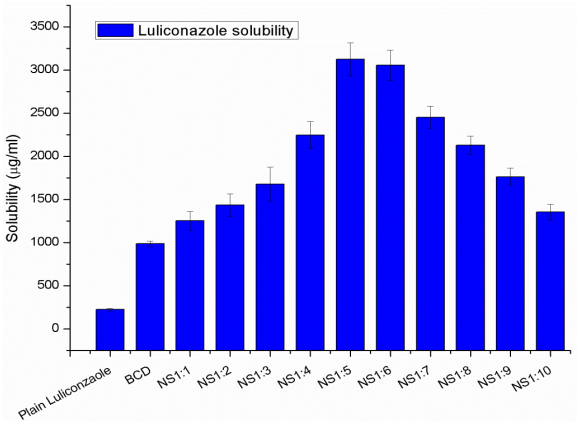

Fig. 1: Solubilization efficiency of NS, all the values were expressed in mean±SD, n=3

Table 1: The experimental matrix-definitive screening design

Run	Factor 1	Factor 2	Factor 3	Factor 4	Response 1	Response 2	Response 3
	A: Molar ratio	B: Volume of solvent (ml)	C: Stirring speed (rpm)	D: Stirring time (min)	Particle size (nm)	Drug loading (%)	EE (%)
1	2	50	4000	2520	110.92	24.32	78.12
2	6	50	3000	2160	65.54	41.56	87.94
3	2	100	2000	2160	203.43	17.56	72.56
4	4	50	2000	2160	135.54	38.45	83.08
5	4	100	4000	2880	176.12	33.78	82.78
6	6	100	4000	2160	167.57	33.17	85.78
7	6	100	2000	2520	190.38	30.45	84.57
8	2	100	3000	2880	152.87	20.32	75.12
9	2	50	2000	2880	134.17	23.26	77.56
10	4	75	3000	2520	108.76	37.12	81.25
11	6	75	2000	2880	149.78	34.33	85.43
12	6	50	4000	2880	93.45	39.78	90.45
13	2	75	4000	2160	134.78	21.58	73.59

Table 2: Statistical analysis of all response models

Source	Sum of squares	Degrees of freedom	Mean square values	F-value	P-Value	
ANOVA of the reduced quadratic model – Particle size						
Model	18469.93	8	2308.74	300.96	<0.0001	Significant
A	482.33	1	482.33	62.88	0.0014	
B	12302.56	1	12302.56	1603.73	<0.0001	
C	1701.98	1	1701.98	221.87	0.0001	
D	0.0221	1	0.0221	0.0029	0.9598	
A^2	82.74	1	82.74	10.79	0.0304	
B^2	122.10	1	122.10	15.92	0.0163	
C^2	3627.09	1	3627.09	472.82	<0.0001	
D^2	1.94	1	1.94	0.2535	0.6411	
Residual	30.68	4	7.67			
Cor Total	18500.62	12				
ANOVA of the reduced quadratic model –Percent drug payload						
Model	788.93	8	98.62	1307.04	<0.0001	Significant
A	522.01	1	522.01	6918.57	<0.0001	
B	102.98	1	102.98	1364.84	<0.0001	
C	7.36	1	7.36	97.57	0.0006	
D	0.0723	1	0.0723	0.9576	0.3832	
A^2	130.55	1	130.55	1730.31	<0.0001	
B^2	0.4988	1	0.4988	6.61	0.0619	
C^2	13.93	1	13.93	184.58	0.0002	
D^2	2.41	1	2.41	31.99	0.0048	
Residual	0.3018	4	0.0755			
Cor Total	789.23	12				
ANOVA of the reduced quadratic model – EE						
Model	378.74	8	47.34	793.20	<0.0001	Significant
A	327.41	1	327.41	5485.61	<0.0001	
B	26.70	1	26.70	447.34	<0.0001	
C	5.66	1	5.66	94.75	0.0006	
D	7.04	1	7.04	117.94	0.0004	
A^2	5.03	1	5.03	84.29	0.0008	
B^2	8.08	1	8.08	135.31	0.0003	
C^2	0.0261	1	0.0261	0.4366	0.5449	
D^2	0.0129	1	0.0129	0.2163	0.6660	
Residual	0.2387	4	0.0597			
Cor Total	378.98	12				

Table 3: Regression equations

S. No.	Response variable	
1	R1	$108.81-6.95A+35.08B-13.05C-0.04D-6.12A^2+7.43B^2+40.51C^2-0.93D^2$
2	R2	$37.11+7.23A-3.21B+0.85C-0.08D-7.69A^2+0.47B^2-2.51C^2+1.05D^2$
3	R3	$81.12+5.72A-1.63B+0.75C+0.83D-1.51A^2+1.91B^2-0.10C^2+0.07D^2$

Table 4: The model fit statistics of all the responses

S. No.	Response variable	Mean	SD	R^2	Adjusted R^2	Predicted R^2	Adeq precision	% CV
1	R1	140.25	2.77	0.9983	0.9960	0.9797	59.7057	1.97
2	R2	30.44	0.2747	0.9996	0.9989	0.9971	106.04	0.9025
3	R3	81.40	0.2443	0.9994	0.9981	0.9920	88.0284	0.3001

Particle size (R1)

The model's 300.96 F-value indicates significance. Noise has a 0.01% probability of causing this significant F-value. Model terms with P-values under 0.0500 are significant. Model terms A, B, C, A^2, B^2, C^2 are important. Model terms above 0.1000 are insignificant. Model reduction may improve a model with many irrelevant terms (excluding hierarchy terms). The discrepancy between the Predicted R^2 of 0.9797 and the Adjusted R^2 of 0.9950 is less than 0.2. Fig. 2A shows that R1 values match predictions. Adeq Precision measures signal-to-noise. A ratio over 4 is ideal. The signal is good at 59.706. Use this model to navigate the design space. The coefficient estimate shows the expected reaction per unit factor value change while all other factors are constant. Orthogonal designs use the average run response as the intercept. In fig. 2B, a perturbation plot shows how each variable affects R1. The equation shows that A, C, and D negatively affect R1, but B positively affects it. A, B, and C have quadratic effects on R1 at greater levels. Three-dimensional RSM plots and contour plots show the interacting influence of variables A and B (fig. 2C and 2D).

Percent drug payload (R2)

The model's 1307.04 F-value indicates significance. Noise has a 0.01% probability of causing this significant F-value. Model terms with P-values under 0.0500 are significant. Here, A, B, C, A^2, C^2, and D^2 are important model terms. Model terms above 0.1000 are insignificant. Model reduction may improve a model with many irrelevant terms (excluding hierarchy terms). The discrepancy between the Predicted R^2 of 0.9971 and the Adjusted R^2 of 0.9989 is less than 0.2. Fig. 3A shows that R2 values match predictions. Adeq Precision measures signal-to-noise. A ratio over 4 is ideal. The signal is good at 106.043. Use this model to navigate the design space. The perturbation plot in fig. 3B shows how each variable affects R2. The equation shows that B negatively affects R2, while A and C positively affect it. A, C, and D have quadratic effects on R2 at increasing levels. Three-dimensional RSM plots and contour plots show the interacting influence of variables A and B (fig. 3C and 3D).

EE (R3)

Model F-value 793.20 indicates significance. A significant F-value owing to noise is 0.01% likely. Sub-0.0500 P-values imply model terms are significant. A, B, C, D, A^2, B^2 are important model terms. The model terms are insignificant if they exceed 0.1000. If your model has many inconsequential terms (excluding hierarchy terms), model reduction may improve it. The Predicted R^2 of 0.9920 and Adjusted R^2 of 0.9981 are within 0.2 for reasonable agreement. R3 values are close to predictions, as illustrated in fig. 4A. Adeq Precision calculates the signal-to-noise ratio. The desirable ratio is over 4. The signal is good at 88.028. Navigate the design space using this model. The perturbation plot in fig. 4B shows how each variable affects R3. In the equation, A, C, and D negatively affect R3, but B positively affects it. Higher values of A and B have quadratic effects on R3. A three-dimensional RSM plot and contour plot show the interactive effect between variables A and B (fig. 4C and 4D).

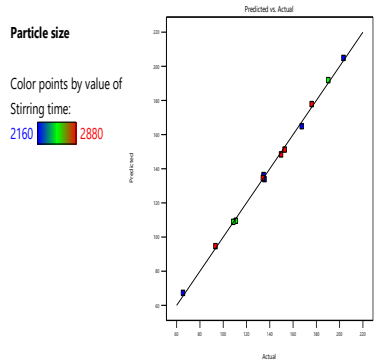

A

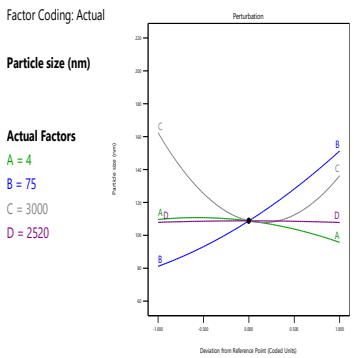

B

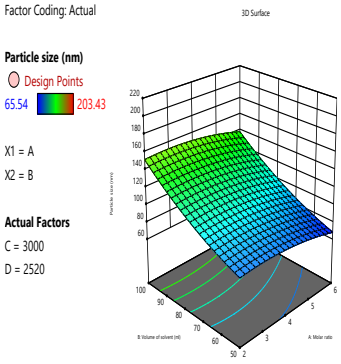

C

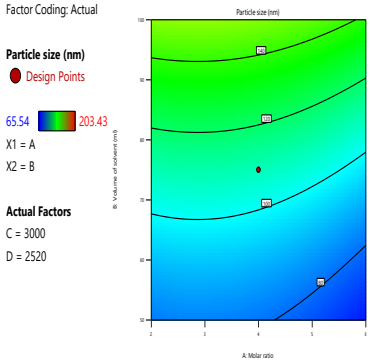

D

Fig. 2: R1-Particle size – (A). Predicted versus actuals (B). Perturbation plot (C) 3D-surface plot (D). Contour plot

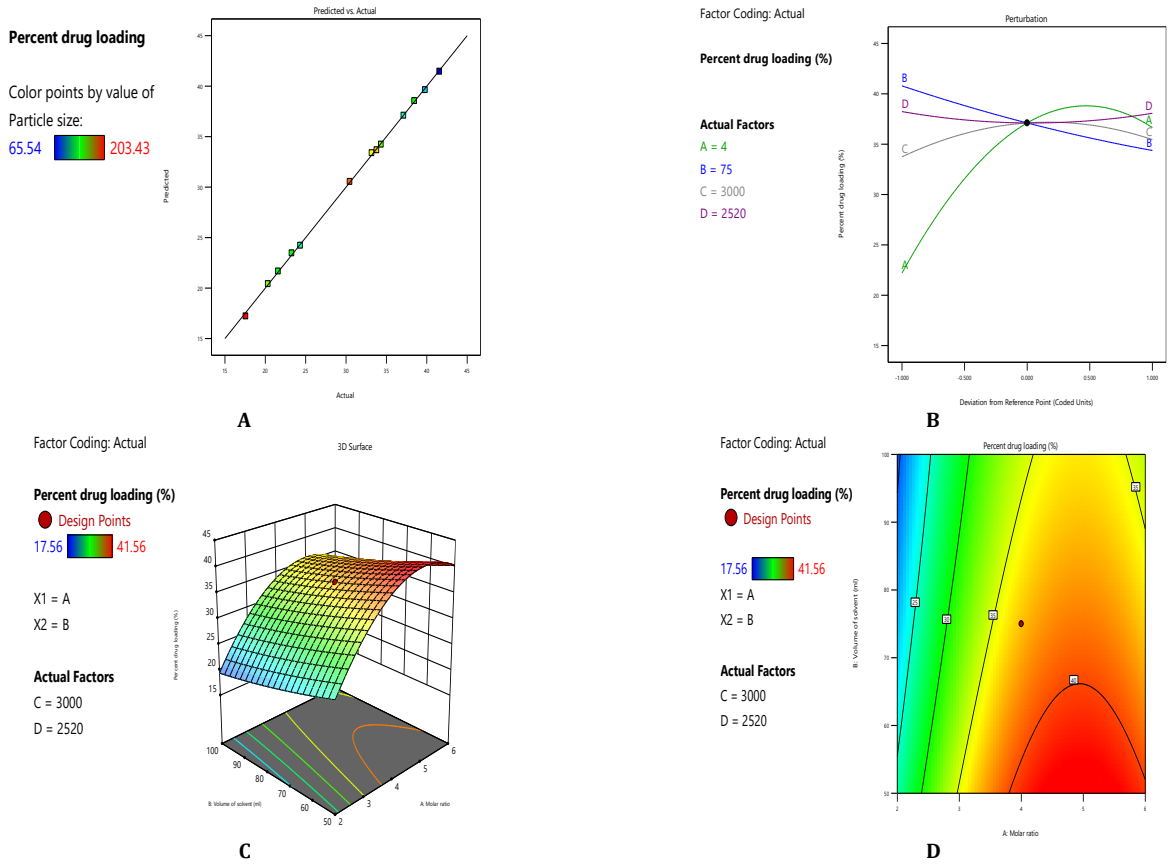

Fig. 3: R2-Percent payload – (A). Predicted versus actuals (B). Perturbation plot (C) 3D-surface plot (D). Contour plot

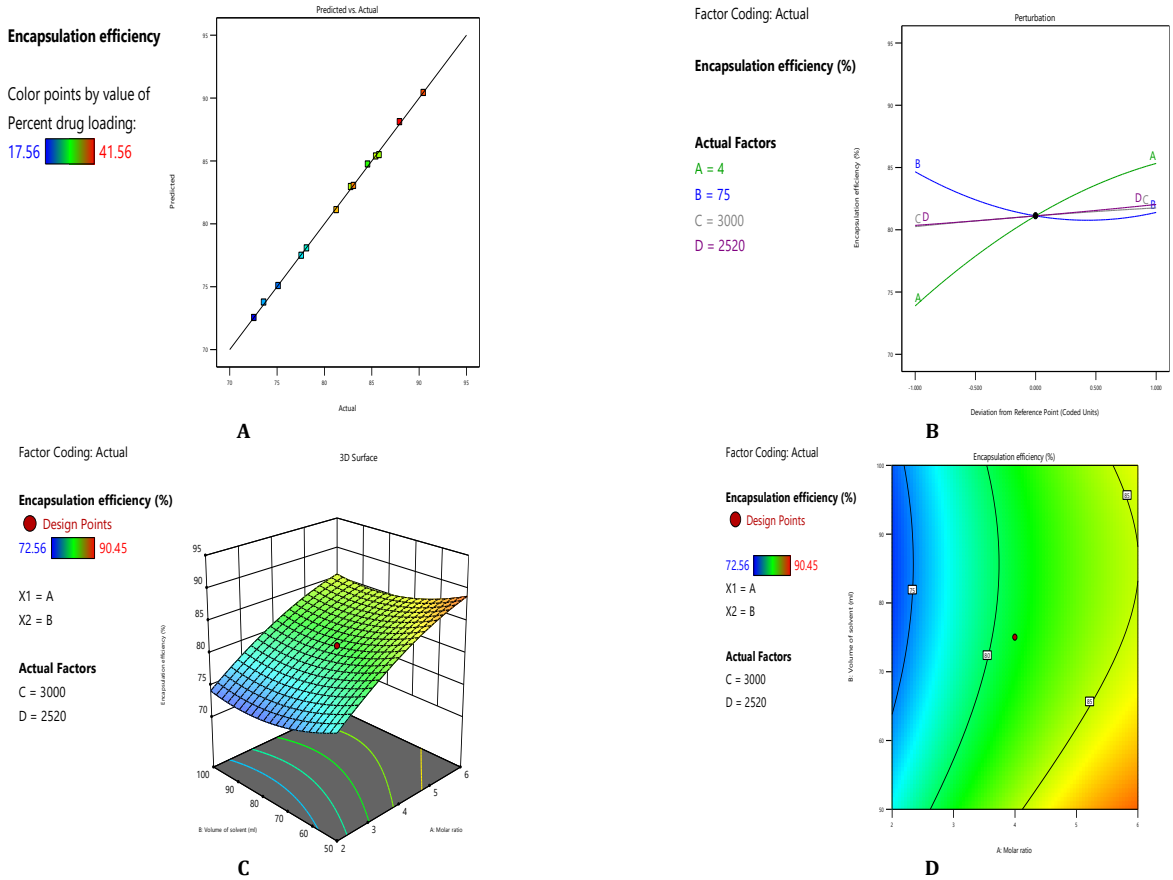

Fig. 4: R3-EE – (A). Predicted versus actuals (B). Perturbation plot (C) 3D-surface plot (D). Contour plot

Using numerical optimization and desirable constraints, the CPPs (A: Molar ratio, B: Volume of solvent, C: Stirring speed, D: Stirring time) that affect particle size, percent drug payload, and EE were optimized. The overlay plot in fig. 5 displays the design space for variables and responses for optimization with a desirability of 0.987. To achieve reliable results, design-space plot chromatographic conditions were chosen as a control method. The optimal technique settings were molar ratio (6), solvent volume (50 ml), stirring speed (3200 rpm), and stirring time (2880 min).

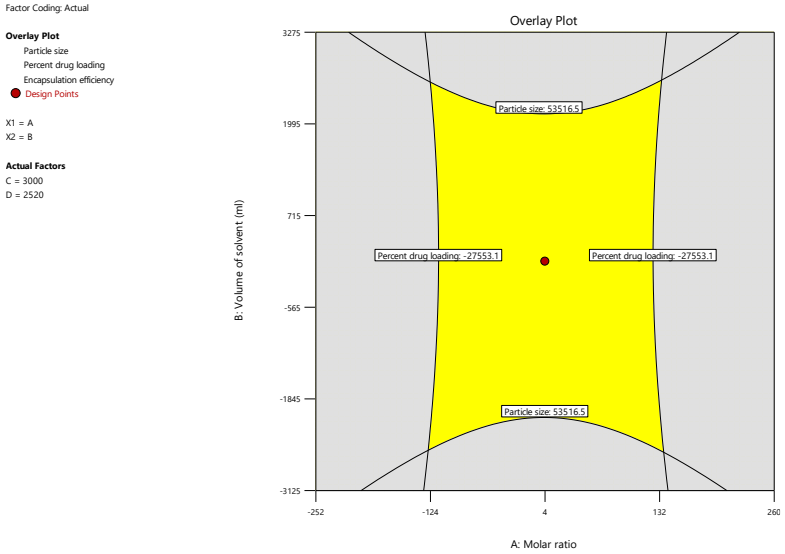

Fig. 5: Overlay plot showing the design space

The optimization process was validated by three tests at optimal critical variable levels. Optimization results suggested using NS6 with a 1:6 molar ratio for drug loading trials. Drug-loaded NS were manufactured under optimal circumstances and tested. Critical approach attribute outcomes matched statistical predictions.

Characterization of LUNS

The average particle size of LUNS evaluated by laser light scattering is 60-73 nm with a lowPDI. Table 5 shows the particle size distribution is unimodal and narrow. Colloidal particles with a narrow PDI are homogeneous. Zeta potential plays a vital function in the interaction of formulation with biological system and it has been reported and proven in various studies till date. It shows the charge type that is present on the NS surface and also provides idea of stability of the prepared formulation in a colloidal suspension. A high ZP indicates stable compounds with minimal agglomeration [10]. All formulas were fine, free-flowing powders. TEM tests indicated that plain NS' normal spherical shape and size remained unchanged after drug encapsulation (fig 6). The particle size of the complexes was compatible with TEM and DLS measurements. Table 5 shows LUNS drug loading and EE.

Table 5: Particle size, PDI, and ZP of plain NS and drug-loaded NS formulation

Sample	Mean particle size±SD (nm)	PDI	ZP (mV)	Drug payload	EE
Plain NS	156.78±3.7	0.18± 0.005	-22.32±2.3	-	-
LUNS1	69.78±2.18	0.26±0.005	-23.42±2.5	41.34±2.13	89.76±0.66
LUNS2	60.58±1.98	0.22±0.005	-21.76±1.9	42.19±1.45	90.12±0.92
LUNS3	72.43±3.15	0.25±0.005	-25.37±2.2	40.98±1.76	89.22±0.53

(All determinations were performed in triplicate and values were expressed as mean±SD, n=3)

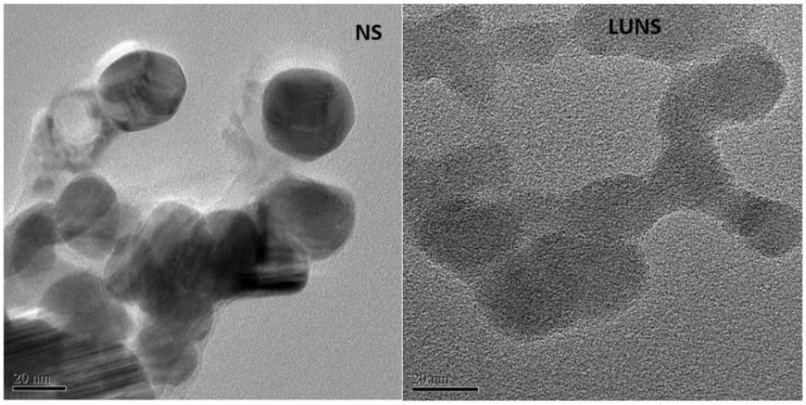

Fig. 6: TEM image of plain NS B. LUNS complexes at 45000 X magnification

FTIR spectra of NS5, LU, and LUNS are compared in fig. 7(A). FTIR investigations demonstrated weak interactions between NS and LU, as drug signals broadened and disappeared in complexes. A comparison of FTIR spectra of LU and complex revealed a significant shift in the fingerprint area (900-1,400 cm−1). LU has main peaks at 3193.98, 3118.76, 3076.33, 3039.69, 2941.32, 2614.36, 2526.64, 2198.76, 1892.09, 1816.87, 1739.72, 1698.56, 1555.12, 1452.33, 1223.17, 958.58, 761.32, and 665.41 cm-1. The formulations enlarged or altered LU characteristic peaks, suggesting NS-LU interactions. Fig. 7(B) shows DSC curves of free LU, plain NS (NS5), and LUNS. LU's DSC spectra exhibited a prominent endothermic peak at 123.66 °C, its melting point. The DSC spectra of NS displayed exothermic peaks at about 350 °C. The LU compound had a broad exothermic peak of about 350 °C. Freeze-dried formulations lost their drug endothermal peak completely. This suggests formulation component interactions. This suggests drug amorphization or inclusion complex development. XRD patterns of pure LU, plain NS (NS5), and LUNS were examined to analyze their physical properties in CDNS. Fig. 7(C) shows LU's high crystalline structure in its characteristic peaks. NS complexes did not show pure LU's peak. LUencapsulated in NSis shown by the absence of crystalline peaks in LUNS6. LU inclusion complexes with NS were validated by FTIR, DSC, and XRD.

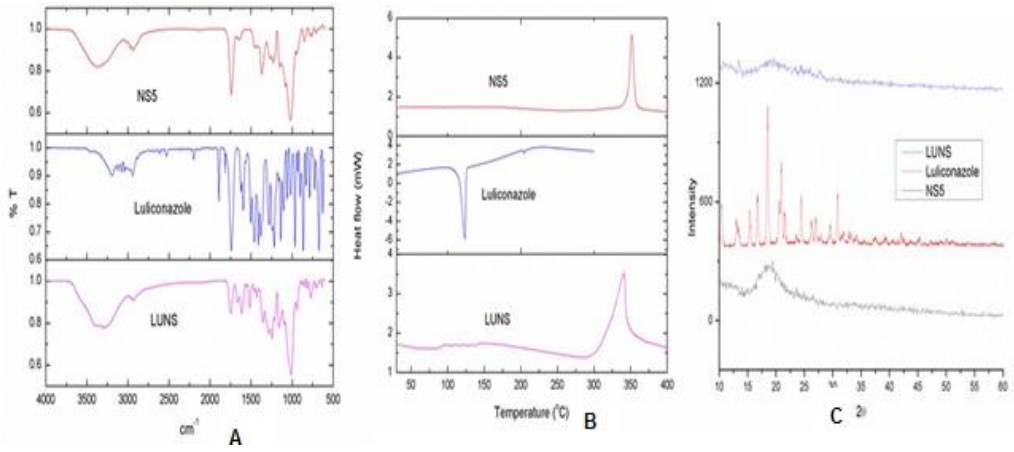

Fig. 7: FTIR (A), DSC (B) and XRD (C) spectra of plain NS, LU and LUNS

Drug release study

Fig. 8 illustrates the dissolution patterns of pure LU and NS complexes in simulated gastric media. *In vitro* release experiments demonstrated that the complex released faster than the pure medication. The medicine encapsulated in NS dissolved faster and better than pure LU, which dissolved only 12% in 12 h. After 12 h, NS formulations released 93-95% LU. The formulated nanosponges showed sustained release of the drug for up to 24 h. Aqueous media's slower dispersion inside the hydrophobic polymer matrix is the cause of the prolonged drug release from the Abemaciclib nanosponges [8].

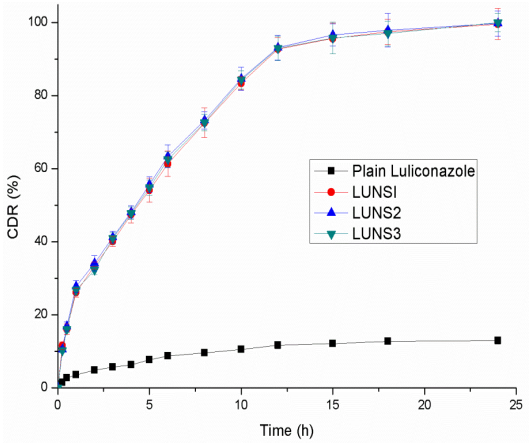

Fig. 8: *In vitro* release of LU from NS, all the values were expressed in mean±SD, n=3

Release kinetics

NS formulation (LUNS3) data was fitted into different kinetic models to identify drug release sequences and mechanisms. Table 6 depicts release kinetics. The first-order model has the highest R2 value (0.9789), showing dose-dependent dynamics. Drugs dissolve and diffuse through the delivery mechanism. Diffusion-controlled drug release occurs when the Higuchi plot has a higher correlation coefficient. Initial drug concentration surpasses matrix solubility. Sink conditions maintain drug diffusion. NS swells a little.

Table 6: Analysis of dissolution pattern

Sample	Zero		First		Higuchi		Korsmeyer Peppas	
	R^2	N	R^2	n	R^2	n	R^2	n
LUNS3	0.8177	4.2543	0.9789	-0.0966	0.9661	22.996	0.9480	63.56

LU gel formulation

A model carbopol gel formulation with LUNS (5, 10, and 15% w/w) was developed. All formulations were non-irritating since their pH ranged from 4.98 to 5.65, which is typical of skin pH 3.0–9.0. LU was evaluated against *Aspergillus fumigatus* and *Candida albicans*. Table 7 indicates inhibition zone mean diameters. LU gel did not suppress *Candida albicans* and *Aspergillus fumigatus* growth in agar diffusion microbiological experiments, whereas NS-based gel did. After 24 h, inhibitory zones reduced microbial growth.

Table 7: Antifungal activity

S. No.	Sample	Zone of inhibition (mm)±SEM
Candida albicans	LUin gel formulation	12.57±1.05
	LUNS1 gel formulation	39.59±2.12
	LUNS2 gel formulation	58.73±2.09
	LUNS3 gel formulation	60.38±2.76
	Marketed formualtion	13.56± 1.07
Aspergillus fumigates	LUin gel formulation	14.32±0.92
	LUNS1 gel formulation	42.34±2.16
	LUNS2 gel formulation	63.78±4.12
	LUNS3 gel formulation	75.78±3.67
	Marketed formualtion	13.8±0.89

All the values were expressed in mean±SD, n=3

Finally, gel formulations retained pH and clarity at room temperature. In 3 mo, LU gel formulation destroyed 18% of the drug (fig. 9). In contrast, LUNS gel formulations did not lose LU content over time. CDNS prevents this.

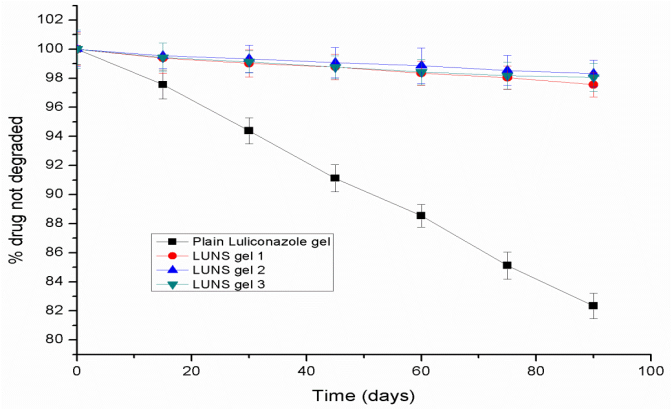

Fig. 9: Results of stability study, All the values were expressed in mean±SD, n=3

CONCLUSION

The study found that freeze-drying can make LUNS. LU was 421.9 mg per g of lyophilized powder. LU's 90% EE suggested an inclusion complex. FTIR, DSC, and XRD indicated LU-NS inclusion complex formation. LUNS diffused faster than pure medicine due to smaller particle size, intermolecular hydrogen bonding, and high-energy amorphous state. After adding NS formulations to a carbopol gel model, skin penetration, antifungal efficacy, and stability were tested. Skin penetration investigations showed NS-encapsulated LU released slowly over 12 h on rat skin. Free LU gel diffused 20 times less than NS. Antifungal activity is four to five times higher than free LU gel. NS-based gel formulation significantly reduced LU's chemical instability after three months of storage at ambient temperature and in the dark. Results show that the CDNS-based gel formulation of LU has tremendous topical administration potential due to its delayed and uniform drug release, increased skin penetration, and superior storage stability.

ACKNOWLEDGEMENT

The writers are grateful to the administration and faculty of the Department of Pharmaceutics, SRM College of Pharmacy, SRMIST, Kattankulathur, Tamilnadu, India. for making the necessary accommodations for their research. The students would also like to express their gratitude for all of the support and encouragement they have given them throughout their time here.

FUNDING

Nil

AUTHORS CONTRIBUTIONS

RA conducted the research, carried out the work plan, and wrote the report. MM reviewed and made revisions to the work. Both authors concur with submitting and publishing. All authors have reviewed and consented to the final version of the paper that has been published.

CONFLICT OF INTERESTS

The authors affirm the absence of any actual, possible, or perceived conflicts of interest in this research.

REFERENCES

1. Khanna D, Bharti S. Luliconazole for the treatment of fungal infections: an evidence-based review. Core Evid. 2014 Sep;9:113-24. doi: 10.2147/CE.S49629, PMID 25285056.
2. Koga H, Nanjoh Y, Kaneda H, Yamaguchi H, Tsuboi R. Short-term therapy with luliconazole a novel topical antifungal imidazole in guinea pig models of tinea corporis and tinea pedis. Antimicrob Agents Chemother. 2012 Jun;56(6):3138-43. doi: 10.1128/AAC.05255-11, PMID 22391525.
3. Subair TK, Mohanan J. Development of nano-based film-forming gel for prolonged dermal delivery of luliconazole. Int J Pharm Pharm Sci. 2022 Feb;14(2):31-41. doi: 10.22159/ijpps.2022v14i2.43253.

4. Gunasheela S, Chandrakala V, Srinivasan S. Development and evaluation of microsponge gel of an antifungal drug. Int J Curr Pharm Res. 2023 Jan;15(1):30-41.
5. Maurya VK, Kachhwaha D, Bora A, Khatri PK, Rathore L. Determination of antifungal minimum inhibitory concentration and its clinical correlation among treatment failure cases of dermatophytosis. J Family Med Prim Care. 2019 Aug;8(8):2577-81. doi: 10.4103/jfmpc.jfmpc_483_19, PMID 31548935.
6. Dogra S, Shaw D, Rudramurthy SM. Antifungal drug susceptibility testing of dermatophytes: laboratory findings to clinical implications. Indian Dermatol Online J. 2019 Mar;10(3):225-33. doi: 10.4103/idoj.IDOJ_146_19, PMID 31149563.
7. Kumar M, Shanthi N, Mahato AK, Soni S, Rajnikanth PS. Preparation of luliconazole nanocrystals loaded hydrogel for improvement of dissolution and antifungal activity. Heliyon. 2019 May;5(5):e01688. doi: 10.1016/j.heliyon.2019.e01688, PMID 31193099.
8. Vivek D, Nishant B, Nikita G, Kajal T. Herbal ethosomal gel containing luliconazole for productive relevance in the field of biomedicine. Vol. 10(3). Biotech Publishing; 2020 Mar. p. 97.
9. Kaur M, Singh K, Jain SK. Luliconazole vesicular-based gel formulations for its enhanced topical delivery. J Liposome Res. 2020 Apr;30(4):388-406. doi: 10.1080/08982104.2019.1682602, PMID 31631734.
10. Lee BC, Pangeni R, Na J, Koo KT, Park JW. Preparation and *in vivo* evaluation of a highly skin and nail-permeable efinaconazole topical formulation for enhanced treatment of onychomycosis. Drug Deliv. 2019 Jan;26(1):1167-77. doi: 10.1080/10717544.2019.1687612, PMID 31738083.
11. Neofytos D, Avdic E, Magiorakos AP. Clinical safety and tolerability issues in use of triazole derivatives in management of fungal infections. Drug Healthc Patient Saf. 2010;2:27-38. doi: 10.2147/dhps.s6321, PMID 21701616.
12. Moskaluk AE, Vande Woude S. Current topics in dermatophyte classification and clinical diagnosis. Pathogens. 2022 Sep;11(9):957. doi: 10.3390/pathogens11090957, PMID 36145389.
13. Volkova TV, Simonova OR, Perlovich GL. New antifungal compound: impact of cosolvency micellization and complexation on solubility and permeability processes. Pharmaceutics. 2021 Nov;13(11):1865. doi: 10.3390/pharmaceutics13111865, PMID 34834280.
14. Tiwari G, Tiwari R, Rai AK. Cyclodextrins in delivery systems: applications. J Pharm Bioallied Sci. 2010 Feb;2(2):72-9. doi: 10.4103/0975-7406.67003, PMID 21814436.
15. Mamatha P, Bhikshapathi DV. Determination of *in vitro* cytotoxicity of entrectinib and pemigatinib nanosponges tablets on a 498, mcf-7, and panc-1 cell lines. Int J Pharm Pharm Sci. 2024 Feb;16(2):12-6. doi: 10.22159/ijpps.2024v16i2.49567.
16. Madhavi M, Shiva Kumar G. Preparation and evaluation of iguratimod oral formulation using cyclodextrin nanosponges. Int J Appl Pharm. 2022 May;14(5):78-87. doi: 10.22159/ijap.2022v14i5.45044.
17. Bhagyavathi A, Sai Lakshmi TK, Sahitya DM, Bhavani B. Nanosponges-a revolutionary targeted drug delivery nanocarrier: a review. Asian J Pharm Clin Res. 2023 Apr;16(4):3-9. doi: 10.22159/ajpcr.2023v16i4.46453.
18. Darandale SS, Vavia PR. Cyclodextrin based nanosponges of curcumin: formulation and physicochemical characterization. J Incl Phenom Macrocycl Chem. 2013 Apr;75(3-4):315-22. doi: 10.1007/s10847-012-0186-9.
19. Rajewski J, Dobrzynska Inger A. Application of response surface methodology (RSM) for the optimization of chromium(III) synergistic extraction by supported liquid membrane. Membranes (Basel). 2021 Nov;11(11):854. doi: 10.3390/membranes11110854, PMID 34832083.
20. Anandam S, Selvamuthukumar S. Fabrication of cyclodextrin nanosponges for quercetin delivery: physicochemical characterization photostability and antioxidant effects. J Mater Sci. 2014 Dec;49(23):8140-53. doi: 10.1007/s10853-014-8523-6.
21. Swaminathan S, Vavia PR, Trotta F, Cavalli R, Tumbiolo S, Bertinetti L. Structural evidence of differential forms of nanosponges of beta-cyclodextrin and its effect on solubilization of a model drug. J Incl Phenom Macrocycl Chem. 2013 Feb;76(1-2):201-11. doi: 10.1007/s10847-012-0192-y.
22. Nazzal S, Khan MA. Response surface methodology for the optimization of ubiquinone self-nanoemulsified drug delivery system. AAPS PharmSciTech. 2002;3(1):E3. doi: 10.1208/pt030103, PMID 12916956.
23. Anandam S, Selvamuthukumar S. Optimization of microwave assisted synthesis of cyclodextrin nanosponges using response surface methodology. J Porous Mater. 2014 Jun;21(6):1015-23. doi: 10.1007/s10934-014-9851-2.
24. Shivakumar HN, Patel PB, Desai BG, Ashok P, Arulmozhi S. Design and statistical optimization of glipizide loaded lipospheres using response surface methodology. Acta Pharm. 2007 Sep;57(3):269-85. doi: 10.2478/v10007-007-0022-8, PMID 17878108.
25. Pimple S, Manjappa AS, Ukawala M, Murthy RS. PLGA nanoparticles loaded with etoposide and quercetin dihydrate individually: *in vitro* cell line study to ensure advantage of combination therapy. Cancer Nano. 2012;3(1-6):25-36. doi: 10.1007/s12645-012-0027-y.
26. Verma P, Pathak K. Nanosized ethanolic vesicles loaded with econazole nitrate for the treatment of deep fungal infections through topical gel formulation. Nanomedicine. 2012 Apr;8(4):489-96. doi: 10.1016/j.nano.2011.07.004, PMID 21839053.
27. Song CK, Balakrishnan P, Shim CK, Chung SJ, Chong S, Kim DD. A novel vesicular carrier transethosome for enhanced skin delivery of voriconazole: characterization and *in vitro/in vivo* evaluation. Colloids Surf B Biointerfaces. 2012 Apr;92:299-304. doi: 10.1016/j.colsurfb.2011.12.004, PMID 22205066.
28. Vicentini FT, Simi TR, Del Ciampo JO, Wolga NO, Pitol DL, Iyomasa MM. Quercetin in w/o microemulsion: *in vitro* and *in vivo* skin penetration and efficacy against UVB-induced skin damages evaluated *in vivo*. Eur J Pharm Biopharm. 2008 Mar;69(3):948-57. doi: 10.1016/j.ejpb.2008.01.012, PMID 18304790.
29. Puglia C, Blasi P, Rizza L, Schoubben A, Bonina F, Rossi C. Lipid nanoparticles for prolonged topical delivery: an *in vitro* and *in vivo* investigation. Int J Pharm. 2008 Feb;357(1-2):295-304. doi: 10.1016/j.ijpharm.2008.01.045, PMID 18343059.
30. Bauer AW, Kirby WM, Sherris JC, Turck M. Antibiotic susceptibility testing by a standardized single disk method. Am J Clin Pathol. 1966 Apr;45(4):493-6. doi: 10.1093/ajcp/45.4_ts.493, PMID 5325707.
31. Chilajwar SV, Pednekar PP, Jadhav KR, Gupta GJ, Kadam VJ. Cyclodextrin based nanosponges: a propitious platform for enhancing drug delivery. Expert Opin Drug Deliv. 2014 Jan;11(1):111-20. doi: 10.1517/17425247.2014.865013, PMID 24298891.
32. Swaminathan S, Cavalli R, Trotta F, Ferruti P, Ranucci E, Gerges I. *In vitro* release modulation and conformational stabilization of a model protein using swellable polyamidoamine nanosponges of β-cyclodextrin. J Incl Phenom Macrocycl Chem. 2010 Mar;68(1-2) :183-91. doi: 10.1007/s10847-010-9765-9.